X-615-69-361
PREPRINT

PHOTOELECTRON FLUX AND PROTONOSPHERIC HEATING DURING THE CONJUGATE POINT SUNRISE

B. C. NARASINGA RAO
E. J. R. MAIER

AUGUST 1969

GODDARD SPACE FLIGHT CENTER
GREENBELT, MARYLAND

PHOTOELECTRON FLUX AND PROTONOSPHERIC HEATING DURING THE CONJUGATE POINT SUNRISE

by

B.C. Narasinga Rao[1] and E.J.R. Maier
Laboratory for Space Sciences
NASA-Goddard Space Flight Center
Greenbelt, Maryland

ABSTRACT: Selected Explorer XXXI data have been studied to establish the extent of protonospheric heating by the onset of photoelectrons from the conjugate ionosphere. Observations made during low latitude passes ($1.2 < L < 2.5$) at altitudes above 2000 km have been analysed to determine the electron and ion temperatures and the flux of photoelectrons for the periods when one foot of the field line is in darkness while the other is undergoing sunrise. In the night hemisphere there is an increase in electron temperature from about 1500 ^{o}K to 3500 ^{o}K and in ion temperature from about 1500 ^{o}K to 3000 ^{o}K and a simultaneous increase in suprathermal flux from about 2×10^{7} el. cm^{-2} sec^{-1} to 15×10^{7} el. $cm^{-2} sec^{-1}$ for electrons of energies greater than 3.7 ev. Observations also show that there is an appreciable return flow of photoelectrons back into the sunlit hemisphere from the conjugate night hemisphere. Theoretical calculations of the energy and flux degradation of the photoelectrons along the field line are made and compared with the observations. Using this photoelectron energy loss as the energy input to the ambient plasma and using the steady state heat conduction equation, the electron temperature profile along the field line is calculated.

---

[1] NRC-NASA Resident Research Associate on leave from the National Physical Laboratory, New Delhi, India.

I. INTRODUCTION

The photoelectrons produced by the ionization of atmospheric neutral particles by solar ultraviolet radiations have energies ranging from a few ev up to about 50 ev. (Dalgarno et al. 1963, Tohamatsu et al 1965). While most of the photoelectrons produced below about 300 km lose their energy locally through elastic and inelastic collisions with neutrals, those produced above that level and those that reach that level from below can escape the local ionosphere, travel along the geomagnetic field lines, and reach the conjugate ionosphere. Hanson (1963) first pointed out that the mean free path of the fast photoelectrons at altitudes above 300 km becomes larger than the atmospheric scale height and hence they may be able to escape into the outer ionosphere. Nisbet (1968) has recently treated this problem of photoelectron escape in more detail and calculated the escape fluxes. As these photoelectrons travel from one hemisphere to the other they lose their energy mainly through elastic collisions with ambient thermal electrons and serve as a heat source for the thermal plasma. (Hanson 1963, Geisler and Bowhill 1965). The effects of these nonlocal photoelectrons were observed by Cole (1965) as a predawn enhancement of the 6300 A airglow, by Carlson (1966) as a predawn increase in electron temperature, and by Yngvesson and Perkins (1968) as an increase in the intensity of the plasma line component of the Thomsen scattered signal from the ionosphere. Direct measurements of the flux of these photoelectrons were made with retarding potential analysers aboard Explorer 31 by Rao and

Donley (1969). Using the data collected with the same sensors as above, we report here the observations on heating of electrons and ions at altitudes of 2000-3000 km by the conjugate point photoelectrons during the period when the conjugate point is undergoing sunrise. We also present the changes observed in the spectral distribution of the photoelectrons arriving in the dark hemisphere from the conjugate sunlit hemisphere. Our observations show an appreciable predawn increase in electron and ion temperatures simultaneously with the arrival of photoelectrons from the conjugate sunlit hemisphere. We will also theoretically estimate the changes in the flux along the field tube and the resulting temperature profiles in both the hemispheres under steady state conditions.

II. EXPERIMENTAL OBSERVATIONS

The measurements are made with three retarding potential analysers on Explorer 31 which may be referred to as the electron sensor, the ion sensor and the quasi-energetic electron sensor since the main purpose of these probes is to measure the electron temperature (T_e) and density (N_e), the ion temperature (T_i) and density (N_i), and the energetic electron flux (J) respectively. The method of measurement and other experimental details are described elsewhere by Donley (1969) and Maier (1969).

Fig. 1 illustrates the increase in the photoelectron flux in the predawn period. It shows two typical measurements made with the electron probe at about 20^{G}N latitude. The left curve is

obtained before sunrise in the conjugate hemisphere while the right curve is obtained after the sunrise. Notice that the background current at the higher retardation voltages in the right curve is about 5 to 10 times larger than the corresponding current in the left curve. This background current is a measure of the suprathermal flux, which is mainly due to photoelectrons as reported in an earlier paper by Rao and Donley 1969.

In Figs. 2a and 2b are shown the electron and ion temperatures measured with the electron and ion sensors for three passes before local ionospheric sunrise. These refer to northern hemisphere during winter 1965-1966. The solar zenith angle in the southern conjugate end of the field line at 300 km is shown in the figure by χ_s. The corresponding χ in the northern end is always greater than 120° and is not shown in the figure. The bottom curve corresponds to night time in the southern end, the middle curve to the time of sunrise, and the top curve to about one hour after sunrise. It is evident that there is a large predawn temperature increase following the sunrise at the conjugate point. The increase is about $2000^{\circ}K$. The ion temperatures shown in Fig. 2b also exhibit similar variations, although the rise is smaller than that of T_e by about $500^{\circ}K$.

Figs. 3a,b show the integral photoelectron flux for electrons having energies greater than 3.7 ev, 7 ev, 11 ev, 15 ev and 34 ev. The energy levels listed are the retarding potentials with respect to the vehicle and are not corrected to the vehicle potential which is normally about -0.5 volts for these passes. Due to spinning of

the satellite at a nominal period of 20 secs, measurements are available at various probe angles with respect to the magnetic field. By grouping several minutes of data we are able to obtain fairly complete coverage of the angular distribution as shown in figure 3. In the dashed portions of the curves, observations could not be made due to sun shining into the sensor and thus producing photoelectron emission from the grids of the sensors. The measurements made at other times and at other locations in the orbit for similar conditions at these angles justify the extrapolations shown in the diagram. Measurements in Fig. 3a correspond to the pass given in Fig. 2a which is taken about 1 hour after sunrise in the conjugate ionosphere. The photoelectron flux leaving the conjugate ionosphere could not be obtained from the same pass, since the satellite pass over the southern hemisphere did not cover the required location at a proper solar zenith angle condition. Therefore, we have chosen data collected on a different day but for the same solar zenith angles at the two ends of the field line as in Fig. 3a. These curves are shown in Fig. 3b. In these figures the direction of magnetic field is such that 180^{o} represents the upward field direction. We note that in the sunlit hemisphere the flux, particularly at low energies, is large and peaks around 130^{o}. This corresponds to a large component flowing up the field line. In addition there is, surprisingly, an appreciable amount of flux coming downward. The upward component represents the

escaping photoelectron flux while the downward component represents the flux of photoelectrons that are scattered and/or mirrored back. It may be noted that the return (downward) flux is more isotropic than the escaping flux. Fig. 3a shows that in the conjugate night hemisphere the flux is larger around 40^{o} indicating a larger flow down the field line. This means that this amount of flux is arriving on the predawn hemisphere from the conjugate sunlit hemisphere along the field line. Note, however, that the upward flux (in the range 90^{o} to 180^{o}) is not negligible, but show a significant energy flow up the field line. As in the previous case this return component represents flux of photoelectrons scattered or mirrored back.

Remembering that during this period only the ionosphere at the southern end of the field line is sunlit, these measurements clearly demonstrate the flow of escaping photoelectrons from their production level in the southern hemisphere, their arrival in the northern hemisphere, and the existence of an observable return flow from the dark hemisphere.

From the integral fluxes measured at different energies, a differential energy spectrum can be obtained. Since we have measurements only at 5 discrete voltages, the differential spectrum is smoothed to get a continuous spectral distribution from 5.5 ev to 25 ev. The values obtained at the 4 midpoints of the energy intervals are indicated in the smoothed spectral distributions shown in Fig. 4. To extend this spectrum to lower energies the observations made at -5 to -2.5 volts by the electron sensor are

used. Thus Fig. 4 shows the spectral distribution from 3 ev to 25 ev. The dashed curve refers to the escaping photoelectrons from the southern hemisphere at a pitch angle of 50^{o} and an altitude of 1000 Km. The dotted curve refers to arriving photoelectrons in the northern hemisphere at a pitch angle of 40^{o} and an altitude of 2300 Km. These angles are chosen because the flux is large at these angles. The pitch angle at 2300 Km in the northern hemisphere corresponds approximately to the theoretically expected angle for electrons having a 50^{o} pitch angle at 1000 Km in the southern hemisphere (as discussed in the next section). It is evident from these curves that the flux of low energy electrons decreases appreciably during travel from one end to the other of the field line.

III. EQUATIONS GOVERNING THE PHOTOELECTRON INTERACTION WITH THE MEDIUM

A detailed discussion of the photoelectron interaction with neutrals and electrons and ions and the resulting energy loss was given by Dalgarno et al (1963) and Dalgarno et al (1967). Theoretical calculations of the photoelectron heating of the conjugate ionosphere were given by Fontheim et al (1968). While energy loss through collisions with neutrals is important at lower altitudes, at altitudes of 1000 km and above energy loss through elastic collisions with ambient electrons dominates. As our observations pertain to higher altitudes, we are only concerned here with the latter mechanism.

The energy degradation of a photoelectron with energy E and pitch angle α due to elastic collisions with ambient electrons is given by Dalgarno et al (1963)

$$\delta E(E,\alpha) = - \frac{1.95 \times 10^{-12}}{E} \frac{dx}{\cos\alpha} n_e \qquad (1)$$

where n_e is the local ambient electron density and dx is the path length along the field line. This equation is valid for energies greater than 1.5 ev and holds approximately for lower energies. An electron whose energy has decreased to 0.5 ev may be considered part of the ambient electron gas and is omitted from the photoelectron flux. Under the assumption that the collisions are small angle collisions, the magnetic moment of the photoelectron motion is conserved along the path, i.e. $\frac{\sin^2\alpha}{B}$ = constant, where B represents the magnetic field strength.

Representing the geomagnetic field by a dipole field, we have

$$ds = \frac{dx}{\cos\alpha} = \frac{L \sin\theta \, (1 + 3\cos^2\theta)^{\frac{1}{2}} \, d\theta}{\left[1 - \sin^2\alpha_o \left(\frac{1 + 3\cos^2\theta}{1 + 3\cos^2\theta_o}\right)^{\frac{1}{2}} \left(\frac{\sin^6\theta_o}{\sin^6\theta}\right)\right]^{\frac{1}{2}}} \qquad (2)$$

where

ds = path length along the motion of photoelectron

θ = geomagnetic colatitude

L = Equatorial radial distance of field line (McIlwain coordinate)

and θ_o refers to the starting point. In the present case the subscript o refers to the point where observations of the excaping photoelectrons are made (Fig. 3b).

We need the distributions of ambient electrons for computing the energy loss. We can assume diffusive equilibrium along the field line at these heights to compute the electron density.

In a multi-constituent ionosphere having different species of ions, we can estimate the electron density by finding the ion distributions first and then, from the charge neutrality constraint, obtain the electron density as the sum of the ion densities. The ion density $n(x^+)$ under diffusive equilibrium is given by (Bauer 1966)

$$n(x^+) = n_o(x^+) \exp - \int_{z_o}^{z} \{m(x^+) - \frac{T_e}{T_e+T_i} m_+\} \frac{g}{kT_i} \, dz$$

where

$m(x^+)$ = ionic mass

m_+ = mean ion mass

T_e = electron temperature

T_i = ion temperature

k = Boltzmann's constant

g = acceleration due to gravity

z = altitude

In the present calculations T_e and T_i are assumed equal and the temperature is assumed constant. These approximations do not

introduce appreciable error in the computation of electron density since the scale height is of the order of 3000 km which is about half the arc length of the field line in the present case. The ion densities at 1000 km as observed by the ion sensor are used as reference values in eq (3) in the calculation of N_e along the field line.

The energy loss of the photoelectrons as they move along the field line can be obtained by combining equations 1, 2 and 3. Under the assumption that none of the escaping photoelectrons can leave the field tube nor those from outside can enter the field tube we may write the flux as:

$$J(E^1, \alpha^1, Z^1) = J(E,\alpha,Z) \frac{\Delta E}{\Delta E^I} \left(\frac{E^1}{E}\right)^{\frac{1}{2}} \frac{A}{A^I} \frac{\Delta\Omega}{\Delta\Omega^I} \qquad (4)$$

where

$J(E,\alpha,Z)$ = photoelectron flux (el. cm^{-2} $sec^{-1}ev^{-1}$ $ster^{-1}$) at energy E for pitch angle α and altitude Z

ΔE = energy increment at Z which becomes ΔE^1 at Z^1

$\Delta\Omega$ = solid angle interval

A = cross sectional area of the field tube

The four ratios on the right hand side of eq (4) arise due to (i) change in the energy increment (ii) change in the energy of the particle (iii) change in the cross sectional area of the field tube, and (iv) change in the solid angle interval due to change in the pitch angle.

Using eq (4) and the photoelectron flux observed in the sunlit hemisphere as given in Fig. 3b, we have calculated the photoelectron flux at 2300 km in the night hemisphere. This is compared with the observed spectrum on the night side in Fig. 4. The important feature is the degradation in the lower energy portion of the spectrum which is seen both in the theoretically calculated and the experimentally observed spectra.

The energy input q_Z per unit volume to the ambient electron gas at any point Z along the field line can now be obtained by combining equations (1) and (4)

$$q_Z = \int_E \int_\alpha \delta E(E,\alpha) . J(E,\alpha,z)\ 2\pi \sin\alpha\ dE\ d\alpha \qquad (5)$$

Using the above equation and the measured photoelectron fluxes given in Fig. (3) we have calculated the energy input along the field tube by numerical intergration.

IV. TEMPERATURE PROFILES IN THE PROTONOSPHERE

The temperature of the electrons is governed by the heat balance equation. The energy loss at these levels through collisions with neutrals and ions is small compared to the loss by the thermal conduction of the electrons (Geisler and Bowhill 1965). Therefore the heat supplied by the photoelectrons increases the temperature which will be eventually limited by thermal conduction. In a steady state situation, the temperature distribution within the protonosphere is governed by the heat conduction equation

$$A\, K_e \frac{dT_e}{ds} = \int_{z}^{z_{Tmax}} A_z . q_z \, ds \qquad (6)$$

where K_e is the electron thermal conductivity, given by

$$K_e = 7.7 \times 10^5 \, T_e^{5/2} \text{ ev cm}^{-1} \text{ sec}^{-1} \text{ deg}^{-1}$$

At sunrise when only one end of the field line is sunlit the position of the temperature maximum may not be over the equator. Using the measured values of T_e on both ends of the field line as boundary conditions, the correct position for T_e max is chosen and the temperature profile along the field line is calculated using equation (6). In these calculations the return photoelectron flux from the night hemisphere (as described in section II) is also taken into account in calculating q_z in eq. (6). The calculated T_e profile for the L = 1.6 field line is shown in Fig. 5. Notice that the gradient of T_e is small for this low L field line. It is only 0.23^o per km at 1000 km in the sunlit side and 0.16^o per km on the night side. The heat flux flowing down through the 1000 km level on the sunlit hemisphere is 8.7×10^8 ev cm^{-2} sec^{-1} while that on the night hemisphere is lower and is equal to 5.8×10^8 ev cm^{-2} sec^{-1}.

V. CONCLUSIONS

The observations presented in this paper demonstrate that during the sunrise period when only one end of the field tube is sunlit, there is a considerable number of photoelectrons flowing into the night hemisphere. There is also an appreciable

flow of photoelectrons from the night hemisphere back toward the sunlit hemisphere. Finally, there is an appreciable pre-dawn temperature increase of the electron-ion gas which is linked to the temperature at the conjugate sunlit hemisphere. The observed photoelectron flux and the electron temperatures have been used to calculate the temperature profile along the field line.

REFERENCES

Bauer, S.J., The constitution of the topside ionosphere, in Electron Density Profiles in Ionosphere and Exosphere, edited by J. Frihagan, p. 270, North-Holland Publishing Company, Amsterdam, 1966.

Carlson, H.C., Ionospheric heating by magnetic conjugate point photoelectrons, J. Geophys. Res. 71, 195, 1966.

Cole, K.D., The predawn enhancement of 6300 A airglow, Ann. Geophys. 21, 156, 1965.

Dalgarno, A., McElroy, M.B. and Moffett, R.J., Electron temperatures in the ionosphere, Planet. Space Sci., 11, 463, 1963.

Dalgarno, A., McElroy, M.B. and Walker, J.C.G., The diurnal variation of ionospheric temperatures, Planet. Space. Sci., 15, 331, 1967.

Donley, J.L., The thermal ion and electron trap experiments on the Explorer 31 satellite, Proc. IEEE, 57, 1061, 1969.

Fontheim, E.G., Beutler, A.E. and Nagy, A.F., Theoretical calculations of the conjugate predawn effects, Ann. Geophys., 24, 389, 1968.

Geisler, J.E. and Bowhill, S.A., Exchange of energy between the ionosphere and the protonosphere, J. Atmos. Terrest. Phys., 27, 1119, 1965.

Hanson, W.B., Electron temperatures in the upper atmosphere, Space Res., 3, 282, 1963.

Maier, E.J.R., Explorer XXXI total current monitor experiments, Proc. IEEE, 57, 1068, 1969.

Nisbet, J.S., Photoelectron escape from the ionosphere, J. Atmos. Terrest. Phys., 30, 1257, 1968.

Rao, B.C.N. and Donley, J.L., Photoelectron flux in the topside ionosphere measured by retarding potential analysers, J. Geophys. Res. 74, 1715, 1969.

Tohmatsu, T., Ogawa, T. and Tsuruta, H., Photoelectronic processes in the upper atmosphere, I. Energy spectrum of the primary photoelectrons, Rep. Ionos. Space Res. Japan, 19, 482, 1965.

Yngvesson, K.O. and Perkins, F.W., Radar Thomson scatter studies of photoelectrons in the ionosphere and Landau damping, J. Geophys. Res., 73, 97, 1968.

CAPTIONS FOR FIGURES

1. Electron probe retardation curves in the predawn period illustrating the increase in the backgroung current and change in the slope of the curves.
2. Electron and ion temperature variations during three satellite passes in the predawn period in the northern hemisphere. Solar zenith angles in the conjugate southern hemisphere at 300 km altitude are shown for each pass. Solar zenith angles at the northern end are greater than 120^{o} for all of these data and are not shown in the figure.
3. Pitch angle distribution of integral photoelectron flux for electrons of different energies observed in the (a) night hemisphere in the predawn period (lower figure) and (b) sunlit hemisphere at sunrise period (upper figure).
4. Smoothed spectral distributions of photoelectrons derived from the observations in the sunlit and night hemispheres. Spectral distribution for the night hemisphere, calculated using the sunlit spectrum, is also shown for comparison.
5. Calculated electron temperature profile along the geomagnetic field line for L = 1.6.

NIGHT HEMISPHERE RETARDATION CURVES

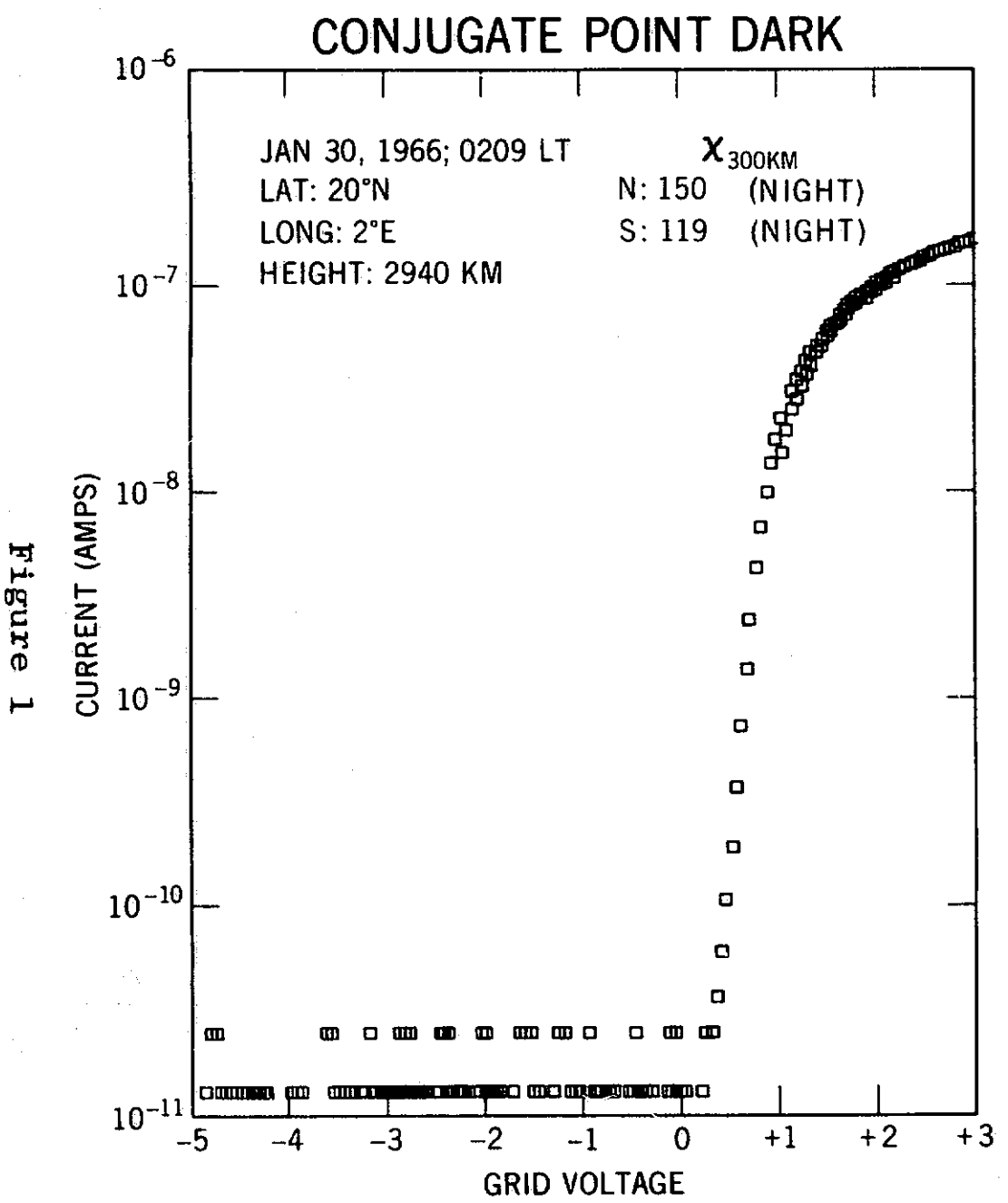

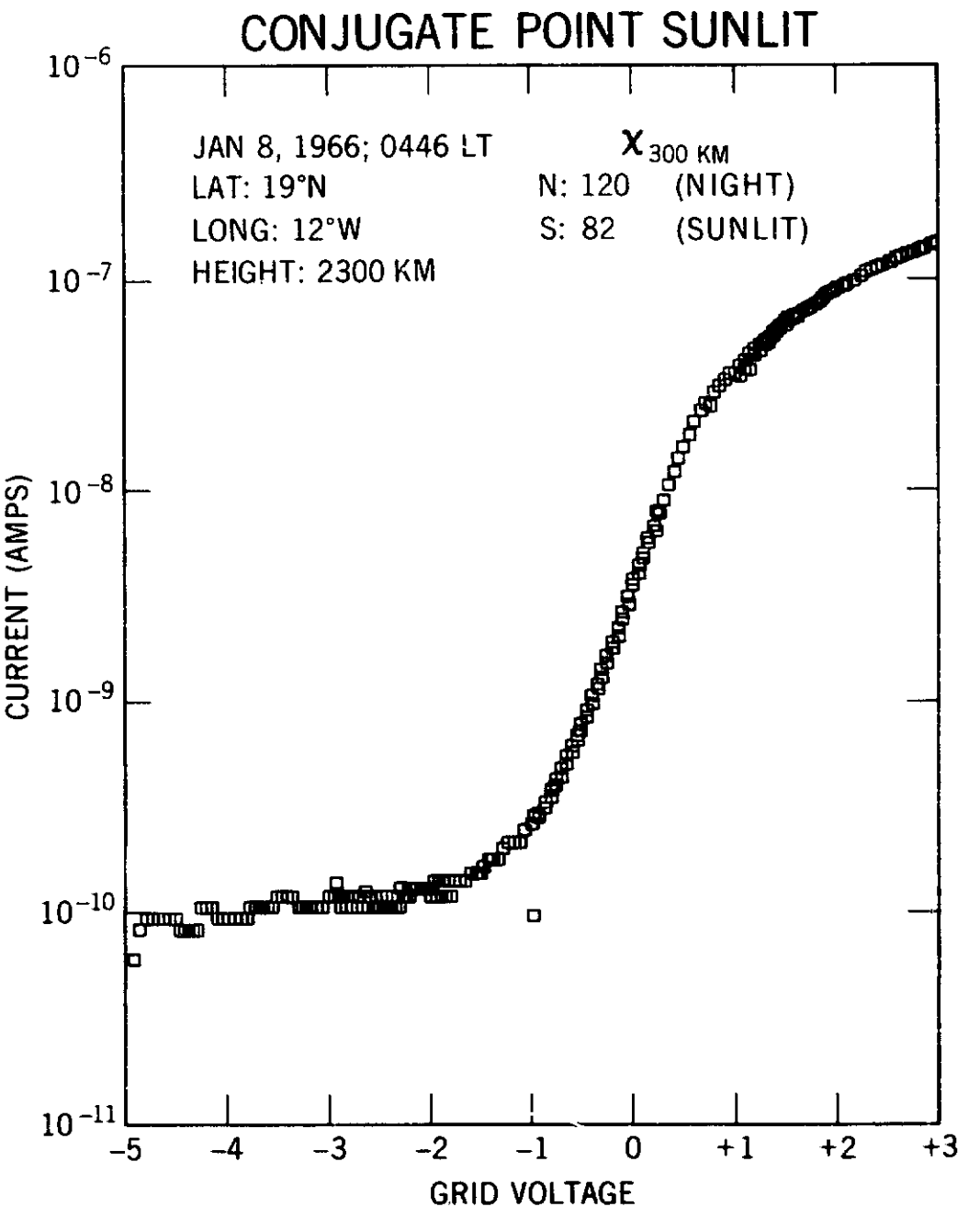

Figure 1

PREDAWN TEMPERATURE RISE IN NORTHERN HEMISPHERE

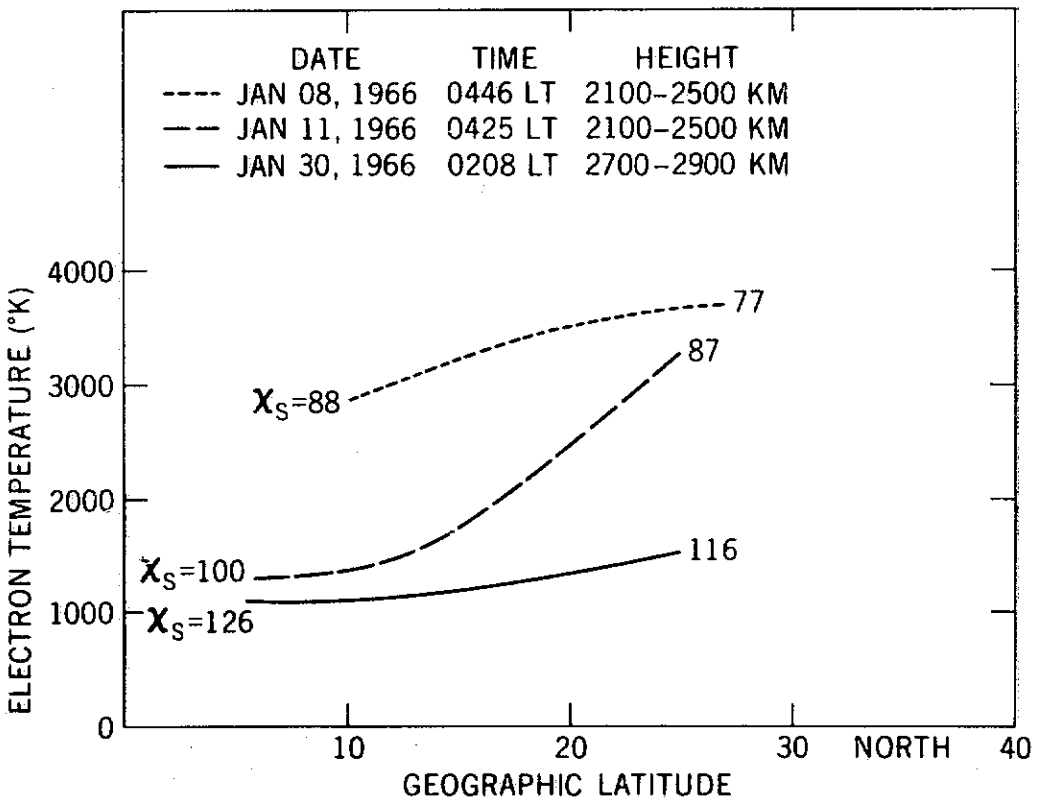

Figure 2

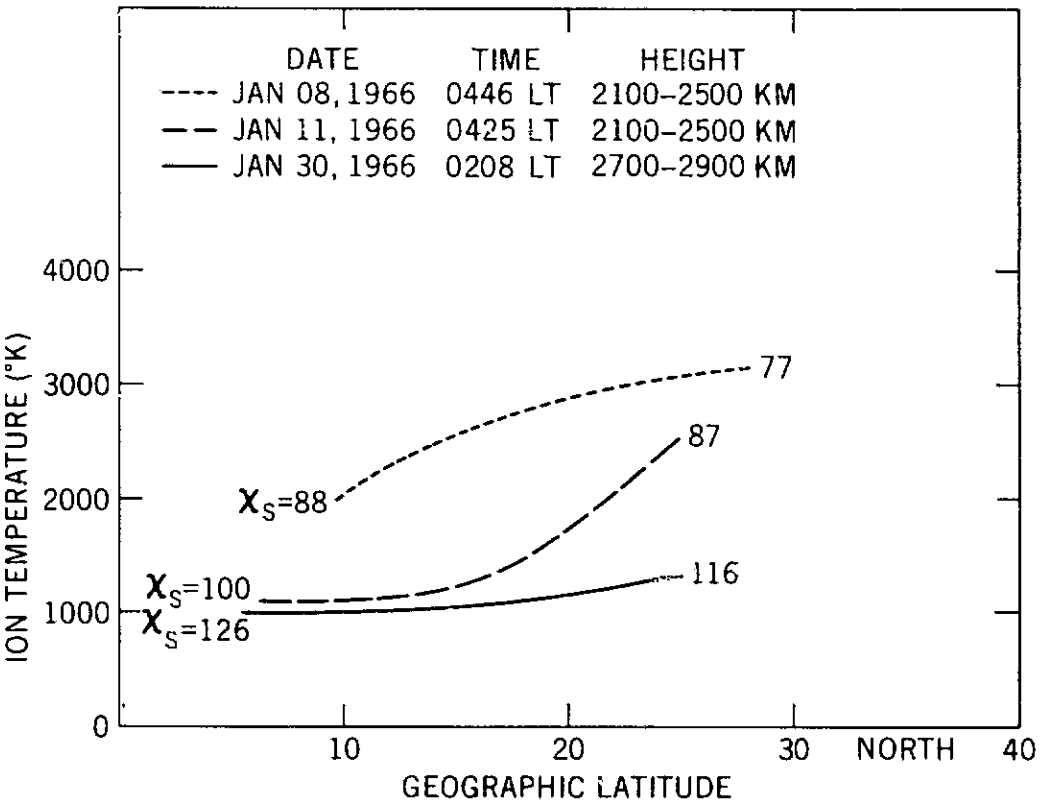

PITCH ANGLE DISTRIBUTION OF PHOTOELECTRON FLUX

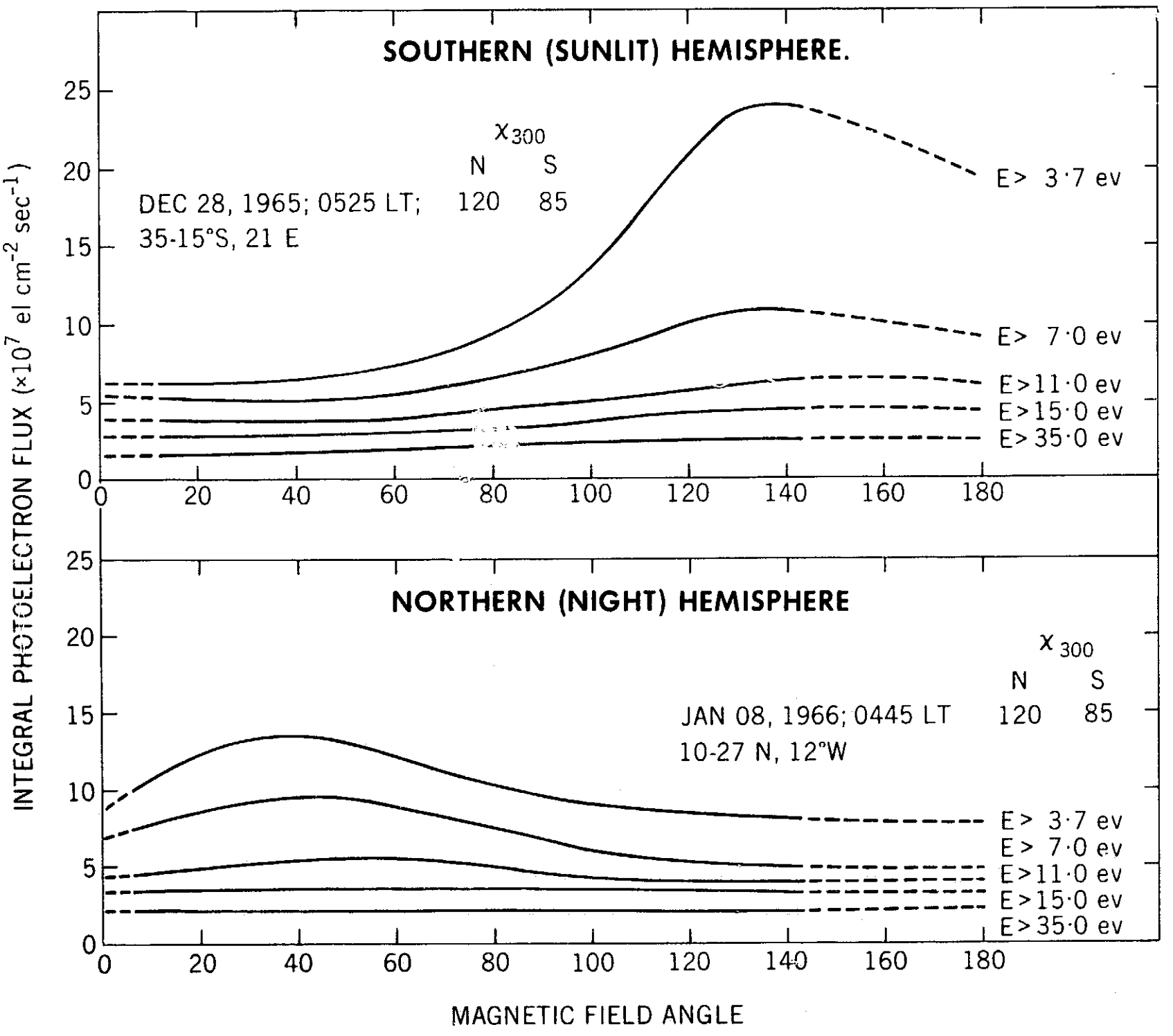

Figure 3

SPECTRAL DISTRIBUTION OF PHOTOELECTRONS IN THE SOUTHERN (SUNLIT) AND NORTHERN (NIGHT) HEMISPHERES

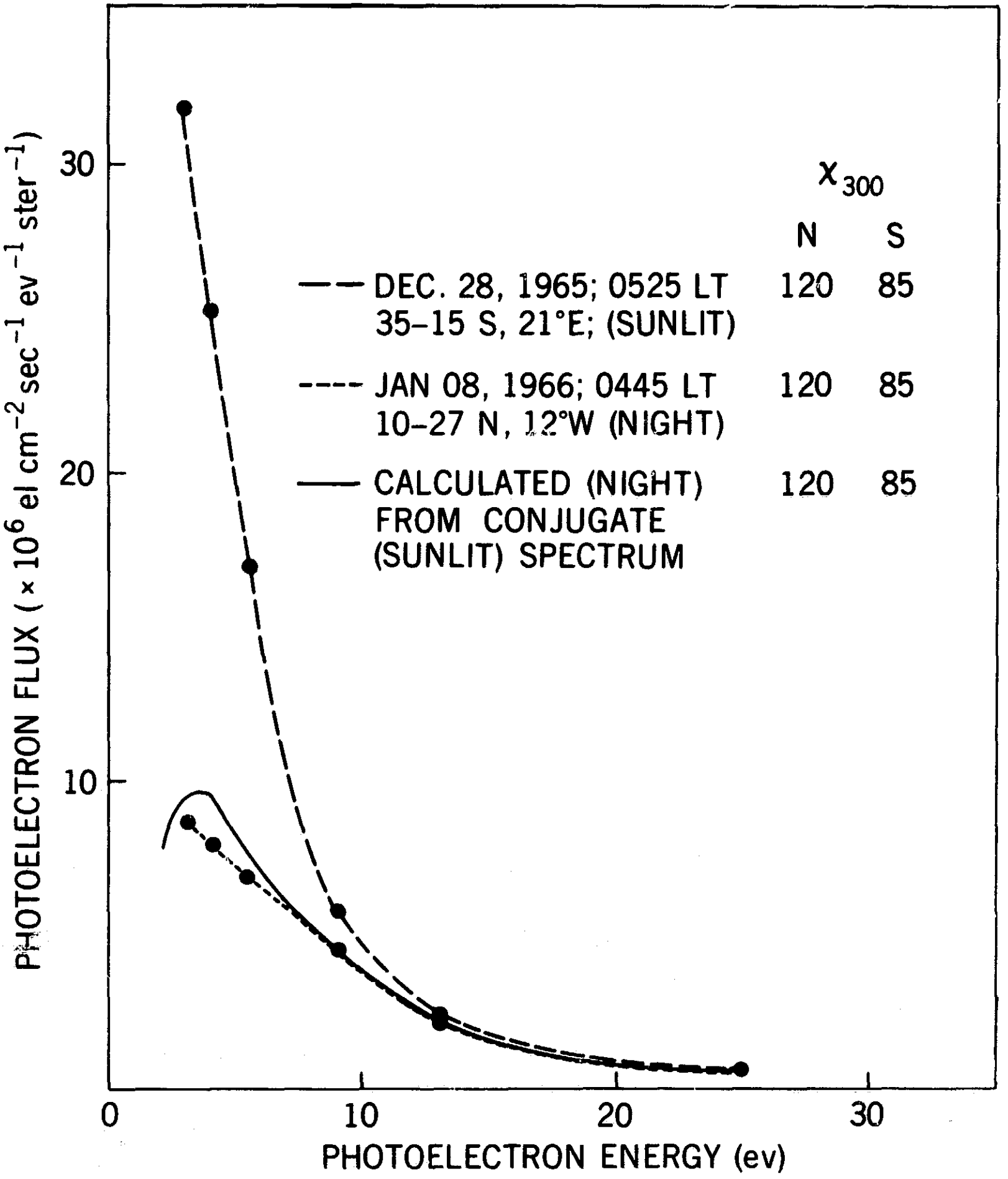

Figure 4

ELECTRON TEMPERATURE PROFILE ALONG MAGNETIC FIELD LINE L = 1.6

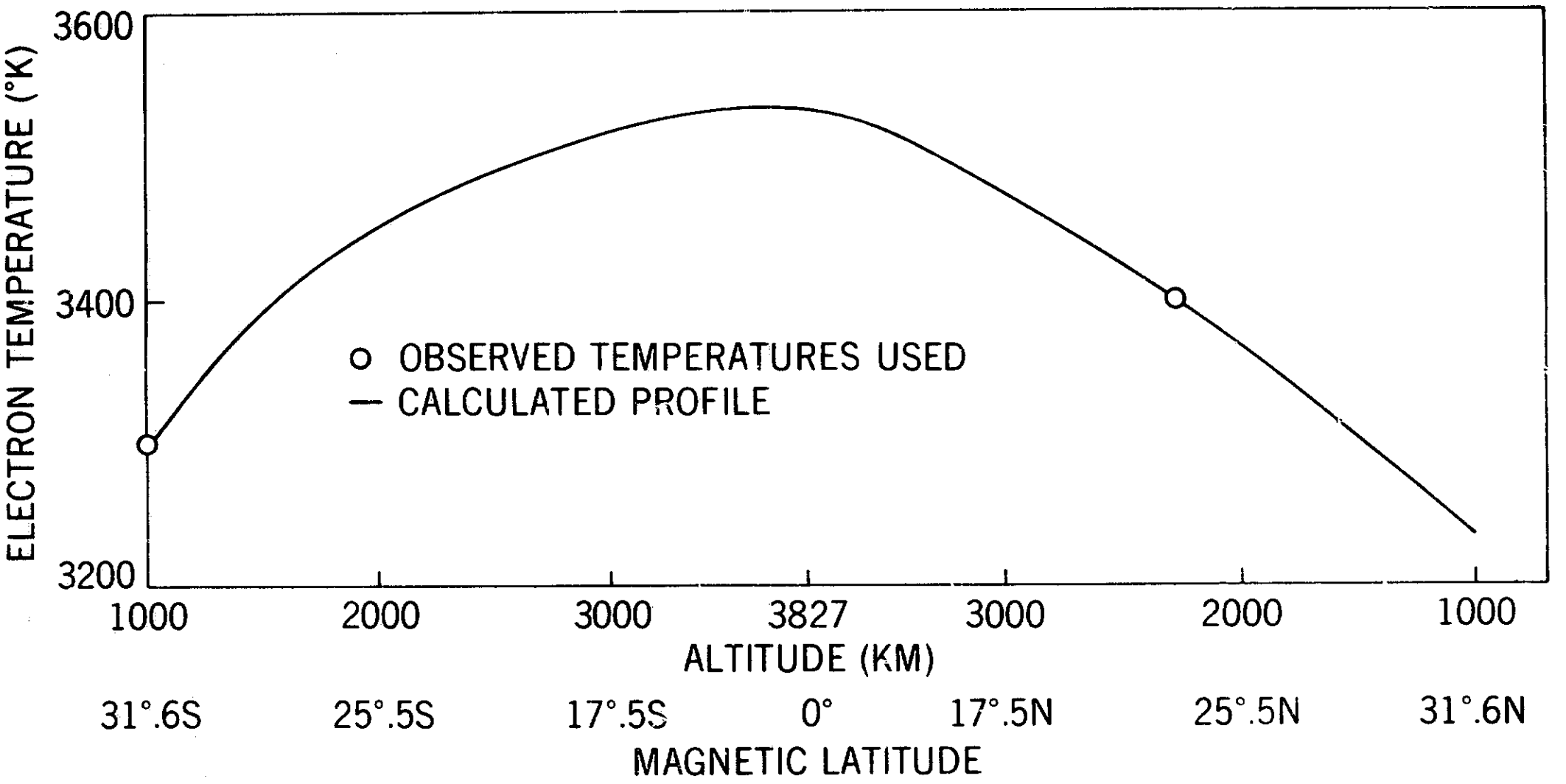

Figure 5